The effects of beam proportion on electromagnetic proton/proton instability and associated ion heating: 2D hybrid simulation

Cite as: Phys. Plasmas **27**, 022901 (2020); https://doi.org/10.1063/1.5128744
Submitted: 23 September 2019 . Accepted: 30 December 2019 . Published Online: 07 February 2020

Jiansheng Yao, Xinliang Gao, Huayue Chen, Yangguang Ke, and Yi Li

Physics of Plasmas ARTICLE scitation.org/journal/php

The effects of beam proportion on electromagnetic proton/proton instability and associated ion heating: 2D hybrid simulation

Cite as: Phys. Plasmas **27**, 022901 (2020); doi: 10.1063/1.5128744
Submitted: 23 September 2019 · Accepted: 30 December 2019 ·
Published Online: 7 February 2020

Jiansheng Yao,[1,2] Xinliang Gao,[1,2,a)] Huayue Chen,[1,2] Yangguang Ke,[1,2] and Yi Li[1,2]

AFFILIATIONS

[1]CAS Key Lab of Geospace Environment, School of Earth and Space Sciences, University of Science and Technology of China, Hefei 230026, China
[2]CAS Center for Excellence in Comparative Planetology, Hefei 230026, China

[a)]Author to whom correspondence should be addressed: gaoxl@mail.ustc.edu.cn

ABSTRACT

In this paper, the effects of beam proportion on the electromagnetic proton/proton instability and involved proton dynamics have been investigated with a two-dimensional hybrid simulation model. The beam proportion is defined as the number density ratio between the beam and all protons. The simulation results show that the saturation amplitude of excited oblique Alfvén waves becomes larger with the increasing proportion of beam protons. Besides, the polarization of oblique Alfvén waves generated by beam protons with a higher proportion tends to be more linear. Moreover, with the increase in the beam proportion, the peak frequencies of excited waves will move toward higher values even exceed the proton gyrofrequency. This will result in more efficient heating of core protons in the perpendicular direction through the cyclotron resonance with Alfvén waves. Our study may provide some new insights into the heating mechanism of the solar wind.

I. INTRODUCTION

In situ measurements of protons' velocity distributions in solar wind, especially when the solar wind has fast flow speed ($v_{SW} > 600\,\mathrm{km/s}$), have shown that there exist two different proton populations.[1–6] The less-dense proton population always referred to as the beam population (denoted with subscript b) drifts relative to the more dense population referred to as the core population (denoted with subscript c) with the velocity of $0 - 3V_A$ parallel to the ambient magnetic field $\boldsymbol{B}_0$, where V_A is the local Alfvén speed. Besides their double-peak velocity distribution, protons are also observed to be gradually cooling due to the expansion of solar wind, but the decline of temperature is much slower than the adiabatic cooling,[4] which suggests some local heating process should take effect during the fast solar wind travels in interplanetary space. Moreover, observations[2–4] have indicated that this heating process is dominant perpendicular to the ambient magnetic field, which results in the common anisotropy of core protons with the perpendicular temperature $T_{\perp c}$ larger than the parallel component $T_{||c}$ in fast solar winds. Observations by Marsch *et al.*[4] show that the temperature anisotropy of core protons $T_{\perp c}/T_{||c}$ is about 3–4 in the fast solar wind near 0.3 AU. However, there is still no consensus on the heating mechanism of core protons. Many mechanisms have been proposed in the literature, including the cascade of turbulence,[7–16] quasi-perpendicular interplanetary shocks,[17,18] Alfvén waves with sufficiently large amplitudes,[19–28] and proton–proton instability.[29–36] In this paper, we focus on the proton– proton instability and associated heating of core protons.

Both theoretical and simulation works have pointed out the obliquely propagating Alfvén wave that will be excited in a low-beta plasma, especially when the relative velocity between beam and core components is a little bit larger than the local Alfvén speed.[33–36] With a two-dimensional (2D) hybrid simulation model, Gao *et al.*[29] first proposed that the core protons can be heated by linearly polarized Alfvén waves generated by the proton–proton instability. In their simulation model, the number density of the beam component n_b was fixed to be 40% of total protons. However, in fact, Ulysses/SWOOPS[5] observations revealed that the proportion of beam component in solar winds is quite variable, ranging from 10% to 45%.

In this study, we have investigated the effects of beam proportion on the proton–proton instability and associated proton heating with a 2D hybrid simulation model. We find both the wave property and

heating efficiency are closely dependent on the beam density. The simulation model is described in Sec. II, the simulation results are illustrated in Sec. III, the summary and discussion are presented in Sec. IV.

II. SIMULATION MODEL

A 2D hybrid simulation model with a periodic boundary condition is performed in this paper. In the hybrid simulation, ions are treated as macroparticles, while electrons are treated as massless fluid.[37–39] The simulation is performed in the x–y plane, and the ambient magnetic field $\boldsymbol{B}_0$ is along the x-axis. According to the observed double-peak distribution of protons, we consider a plasma model containing two proton populations, such as a core population denoted with subscript "c" and a less dense beam component denoted with subscript "b" drifting along the ambient magnetic field in the x-direction. Initially, both beam and core populations satisfy Maxwellian distribution and have the same plasma beta, $\beta_c = \beta_b = 0.01$. The plasma beta of electrons is $\beta_e = 0.01$. The beam population drifts relative to the core population with velocity $\boldsymbol{U_{bc}} = 1.55V_A$ along the x-axis. The beam proportion n_b/n_e ($n_e = n_b + n_c$) measured by Ulysses/SWOOPS varies from 10% to 45%.[5] In this study, we have performed four runs with different n_b/n_e: run 1 with $n_b/n_e = 0.15$, run 2 with $n_b/n_e = 0.25$, run 3 with $n_b/n_e = 0.35$, and run 4 with $n_b/n_e = 0.42$. Other parameters are same in these four runs.

In the simulations, the units of length and time are the proton inertial length $d_i = c/\omega_{pp}$ (where c and ω_{pp} are the light speed and proton plasma frequency, respectively), and the inverse of the proton gyrofrequency Ω_p^{-1}. The plasma velocity is normalized to V_A. The number of grid cells is $n_x \times n_y = 256 \times 256$, and the size of each cell

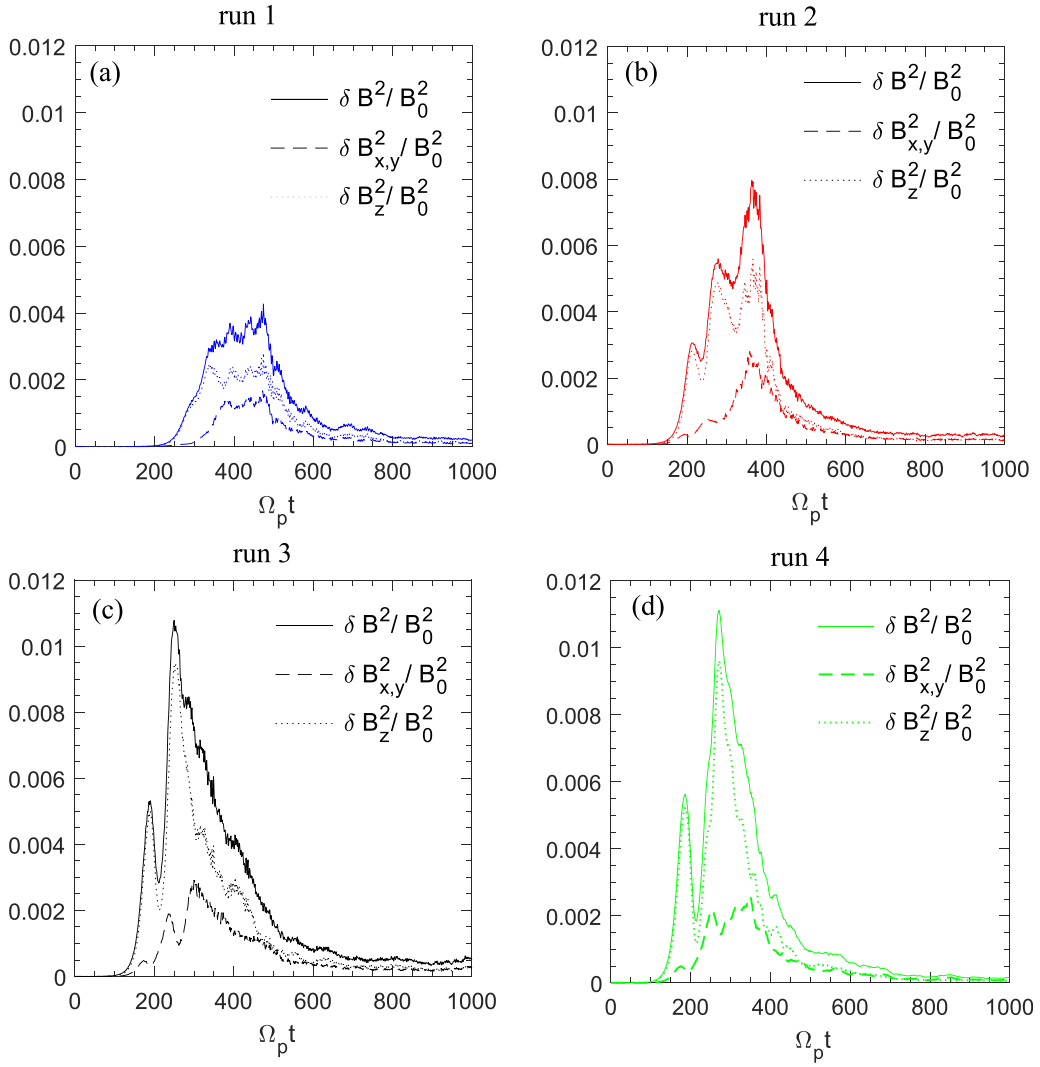

FIG. 1. The time evolution of the amplitudes of fluctuating magnetic field $\delta B^2/B_0^2$ (displayed with solid lines), $\delta B_z^2/B_0^2$ (displayed with dotted lines), and $\delta B_{x,y}^2/B_0^2$ (displayed with dashed lines) (where $\delta B_{x,y}^2/B_0^2 = \delta B_x^2/B_0^2 + \delta B_y^2/B_0^2$) for (a) run 1 with 15% beam protons, (b) run 2 with 25% beam protons, (c) run 3 with 35% beam protons, and (d) run 4 with 42% beam protons, respectively. Run 1, run 2, run 3, and run 4 are displayed with blue lines, red lines, black lines, and green lines respectively.

is $0.8d_i \times 0.8d_i$. The time step is $\Delta t = 0.025\Omega_p^{-1}$. The electron resistive length is set as $L_r = \eta c^2/(4\pi v_A) = 0.02c/\omega_{pp}$. The average proton number in each cell is $n_{pc} = 100$.

III. SIMULATION RESULTS

Figure 1 displays the time evolution of the amplitudes of fluctuating magnetic field $\delta B^2/B_0^2$ (solid lines), $\delta B_z^2/B_0^2$ (dotted lines), and $\delta B_{x,y}^2/B_0^2$ (dashed lines; where $\delta B_{x,y}^2/B_0^2 = \delta B_x^2/B_0^2 + \delta B_y^2/B_0^2$) for run 1 (blue), run 2 (red), run 3 (black), and run 4 (green), respectively. As shown by Fig. 1(a), the instability starts at $\Omega_p t \approx 200$ for run 1 and reaches its saturation at $\Omega_p t \approx 350$ with amplitude $\frac{\delta B^2}{B_0^2} \approx 0.004$. At the saturation time, the ratio between δB_z^2 and $\delta B_{x,y}^2$ is about 1.7, suggesting that the excited Alfvén waves are more circularly polarized. Comparing three runs in Figs. 1(a)–1(d), we find that the instability starts earlier as the proportion of the beam protons increases. The instability begins in run 2, run 3, and run 4 at $\Omega_p t \approx 150$, 100, and 95, respectively. Meanwhile, the saturation amplitude of $\delta B^2/B_0^2$ also increases with the increasing beam proportion, which are 0.004, 0.008, 0.0108, and 0.0112 for run 1, run 2, run 3, and run 4, respectively. Interestingly, it is clearly found that the ratio between δB_z^2 and $\delta B_{x,y}^2$ tends to become larger when the proportion of beam protons increases, meaning the polarization of excited Alfvén waves becomes more linear with a higher beam proportion. The excited linearly polarized Alfvén waves are also observed in the simulation performed by Gao *et al.*,[25] where a large proportion of beam protons (40%) is initialized.

The $k_x - k_y$ diagram obtained from the fast Fourier transform (FFT) of $\delta B_z/B_0$ for run 2 is exhibited in Fig. 2 at three different times. It is worth noting that the evolution of wave numbers exhibits a similar trend in all runs, and so we only present the result for run 2 without any preference. Just as expected, the Alfvén waves are excited with large perpendicular wavenumbers $0.4 < k_y c/\omega_{pp} < 1.8$, whose wave normal angle can reach up to about 60° as shown in Fig. 2(a). With the time evolution ($\Omega_p t = 350$), both k_x and k_y tend to have larger ranges, i.e., $1 < k_x c/\omega_{pp} < 1.4$ and $0 < k_y c/\omega_{pp} < 1.8$, but the magnetic power is reduced. At a much later time, as shown in Fig. 2(c), the wave normal angles of Alfvén waves fall below 50°, and the magnetic power decreases to a very low level. This evolution pattern is quite consistent with that shown in Gao *et al.*[29]

The distribution of magnetic power in the $k_x - \omega$ plane for run 1, run 2, run 3, and run 4 is illustrated in Figs. 3(a)–3(d), respectively. The frequencies of Alfvén waves in Fig. 3(a) are in the range of $0.6 < \omega/\Omega_p < 0.9$, which are well below the gyrofrequency of proton Ω_p. The peak frequency of wave modes is $\omega \approx 0.9\Omega_p$, and the corresponding parallel wavenumber is $k_x c/\omega_{pp} \approx 1.4$. Comparing four runs, we find that the peak frequency of excited waves will move toward higher values, even exceed the proton gyrofrequency (run 3 and run 4) when the beam proportion increases. The highest frequencies are $\omega \approx 1.1\Omega_p$ and $\omega \approx 1.18\Omega_p$ for run 3 and run 4, respectively. The parallel wavenumbers corresponding to these frequencies are $k_x c/\omega_{pp} \approx 1.5$ and $k_x c/\omega_{pp} \approx 1.6$, respectively.

We also utilized the open source code "BO"[40] (http://code.ennresearch.com/bo/) to calculate the dispersion relation and linear growth rate.[41,42] The wave normal angle will be fixed at $\theta = 60°$ for simplicity, since this is the wave normal angle of the dominant wave mode in our simulation. The linear growth rates [Fig. 4(a)] and dispersion relations [Fig. 4(b)] for different runs are illustrated in Fig. 4. It is clearly shown that, with the increase in the beam proportion, the growth rate and peak frequency also increase. Note that the frequency of wave modes in Fig. 4(b) is always smaller than the proton gyrofrequency. Moreover, the evolution of k_x (not shown) shows that the wave modes having frequencies over gyrofrequency are excited after the linear phase, which may be caused by the coupling between Alfvén waves and low-frequency density fluctuations. As demonstrated by the previous work,[43] Alfvén waves with an incoherent spectrum will drive low-frequency density fluctuations via pondermotive force.

Since the wave properties are closely dependent on the beam proportion, we have also investigated its effect on the associated proton heating involved in the instability. The temporal profiles of the temperature of core protons are shown in Fig. 5. The blue, red, and black lines correspond to the temperature of core protons in run 1, run 2, and run 3, respectively. The solid lines and dashed

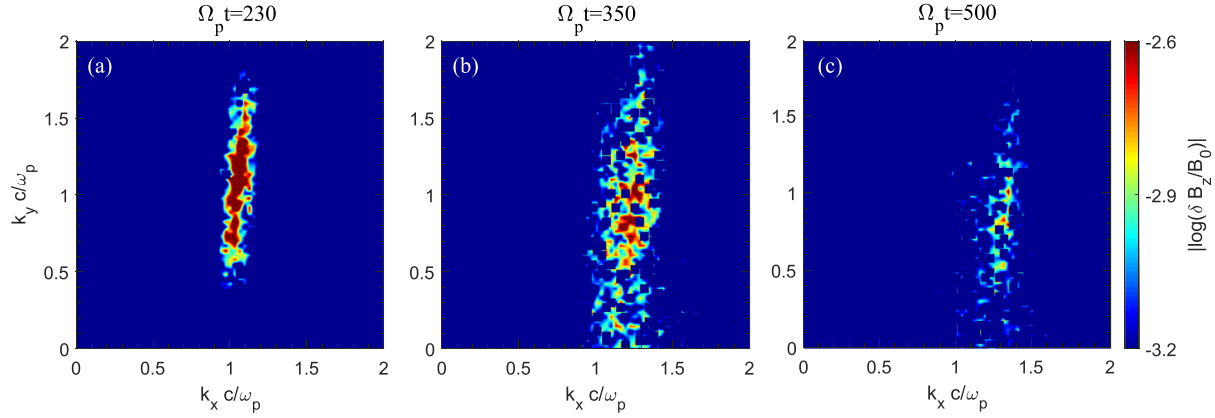

FIG. 2. The $k_x - k_y$ diagram via the fast Fourier transform (FFT) of $\delta B_z/B_0$ for run 2 at different times. (a) $k_x - k_y$ diagram of $\delta B_z/B_0$ at $\Omega_p t = 230$, (b) $k_x - k_y$ diagram of $\delta B_z/B_0$ at $\Omega_p t = 350$, and (c) $k_x - k_y$ diagram of $\delta B_z/B_0$ at $\Omega_p t = 500$. These three times correspond to the growth stage, saturation stage, and decay stage for run 2, respectively.

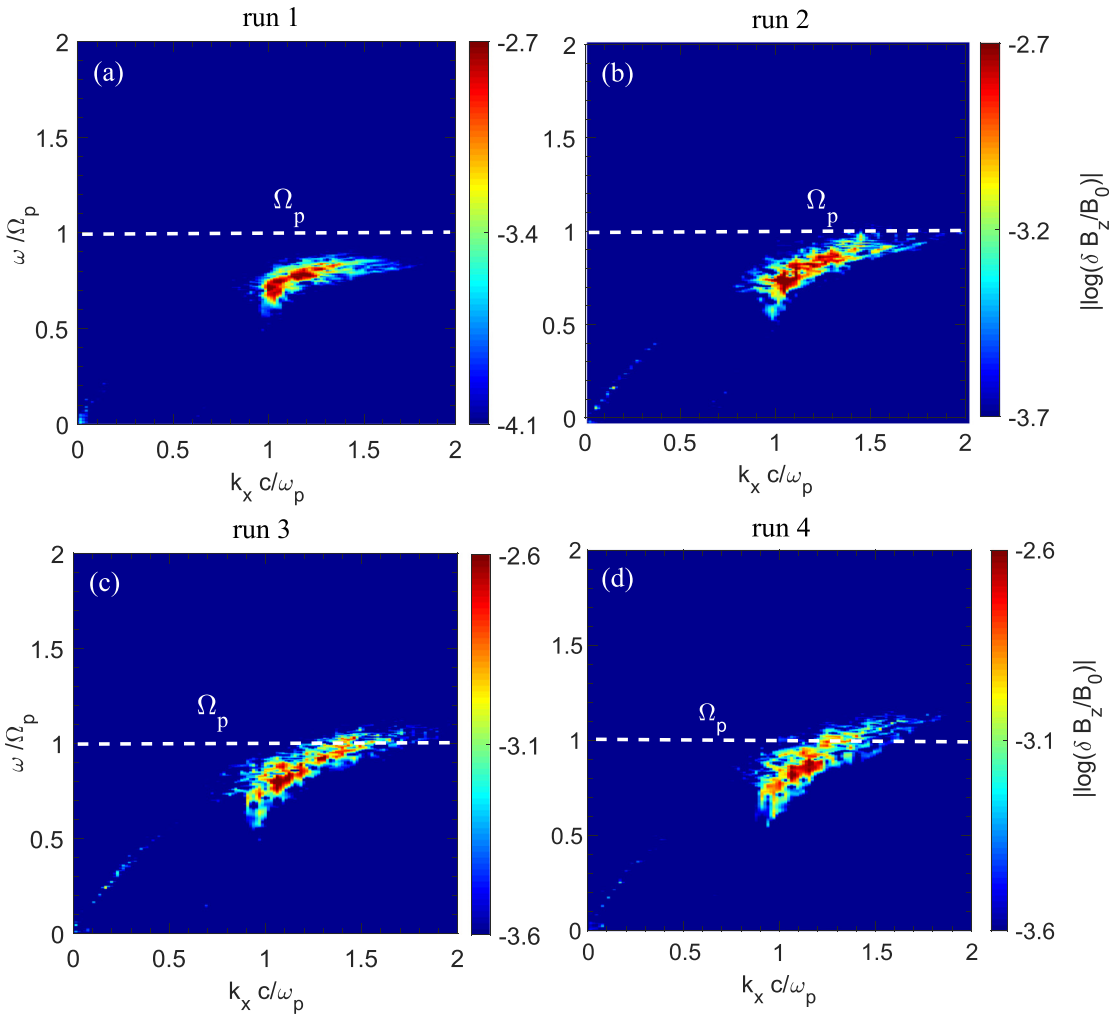

FIG. 3. (a) The magnetic power in $k_x - \omega$ plane for run 1. (b) The magnetic power in $k_x - \omega$ plane for run 2. (c) The magnetic power in $k_x - \omega$ plane for run 3. (d) The magnetic power in $k_x - \omega$ plane for run 4. In all panels, the white dashed lines denote the gyrofrequency of the proton.

lines denote perpendicular temperature and parallel temperature, respectively. The parallel and perpendicular temperatures are calculated following this procedure:[19] first, we calculate the parallel temperature $T_{j||} = m_j/k_B\ \langle(v_{||j} - \langle v_{||j}\rangle)^2\rangle$ and the perpendicular temperature $T_{j\perp} = \frac{m_j}{2k_B}\langle(v_{\perp 1j} - \langle v_{\perp 1j}\rangle)^2 + (v_{\perp 2j} - \langle v_{\perp 2j}\rangle)^2\rangle$ for ion species j (i.e., core protons and beam protons in our simulation) in every grid cell (the bracket $\langle\rangle$ denotes an average over one grid cell), where $v_{||j} = v_{xj}$, $v_{\perp 1j} = v_{yj}$, $v_{\perp 2j} = v_{zj}$, and k_B is Boltzmann constant; then, the temperatures are averaged over all grids. Using this method, the effect of the bulk velocity at each location on the temperature can be eliminated. As shown in Fig. 4, with the increase in the proportion of beam protons, the perpendicular temperature of core protons increases at an earlier time and reaches a larger value. The perpendicular temperature of core population for run 1, run 2, run 3, and run 4 begins to increase at $\Omega_p t \approx 220$, $\Omega_p t \approx 120$, $\Omega_p t \approx 90$, and $\Omega_p t \approx 85$, respectively, which is consistent with the beginning of instability in Fig. 1. When perpendicular temperatures of core protons in different runs reach their peaks, the anisotropies in four runs are $T_{c\perp}/T_{c0} \approx 1.5$, $T_{c\perp}/T_{c0} \approx 2.7$, $T_{c\perp}/T_{c0} \approx 4$, and $T_{c\perp}/T_{c0} \approx 4.3$, respectively.

With the same format, the final velocity distributions in the $v_{||c} - v_{\perp c}$ plane for run 1, run 2, run 3, and run 4 at $\Omega_p t \approx 1000$ are presented in Figs. 6(a)–6(d), respectively. The initial velocity distribution of the core population for four runs satisfies Maxwellian distribution. While, after the instability, we can find that some core protons are scattered in the perpendicular direction (Fig. 6). According to Fig. 3(a), the peak frequency and parallel wave number of excited waves are about $0.9\Omega_p$ and $1.4\omega_p/c$, and the critical resonant velocity (vertical magenta line) for protons can be estimated as $-0.07v_A$ according to the resonant condition $\omega - k_{||c}v_{||c} = \Omega_p$. In Fig. 6(b), it is clearly shown that the excited Alfvén waves can only heat protons with velocities smaller than $-0.07v_A$, supporting that the heating mechanism should be the

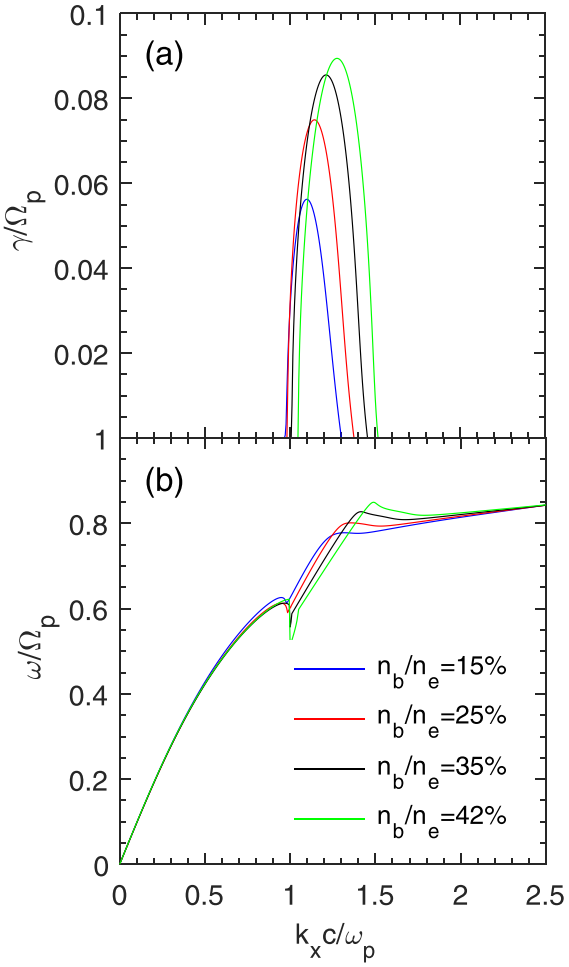

FIG. 4. (a) The growth rates and (b) the dispersion relations for waves triggered by different proportions of beam. Here blue lines, red lines, black lines, and green lines correspond to the beam proportion $n_b/n_e = 15\%$, 25%, 35%, and 42%, respectively. The propagating angle of these waves is fixed to be 60°.

cyclotron resonant interactions. As the proportion of beam protons increases, the critical resonant velocity is significantly changed, i.e., $v_{||c} \approx 0$ in run 2, $v_{||c} \approx 0.05v_A$ in run 3, and $v_{||c} \approx 0.12v_A$ in run 4, resulted from the increase in the peak frequency of excited waves. Therefore, more protons are scattered in the perpendicular direction in runs 2, 3, and 4 [Figs. 6(b)–6(d)], which is also consistent with the larger perpendicular temperature shown in Fig. 4.

IV. SUMMARY AND DISCUSSION

In this study, we have investigated the effects of beam proportion on the electromagnetic proton/proton instability and involved proton dynamics with 2D hybrid simulations. We find that the saturation amplitude of excited oblique Alfvén waves becomes larger with the increasing proportion of beam protons. Besides, the polarization of oblique Alfvén waves generated by beam protons with a higher proportion tends to be much more linear. What's more, with the increase in beam proportion, the peak frequencies of excited waves will move

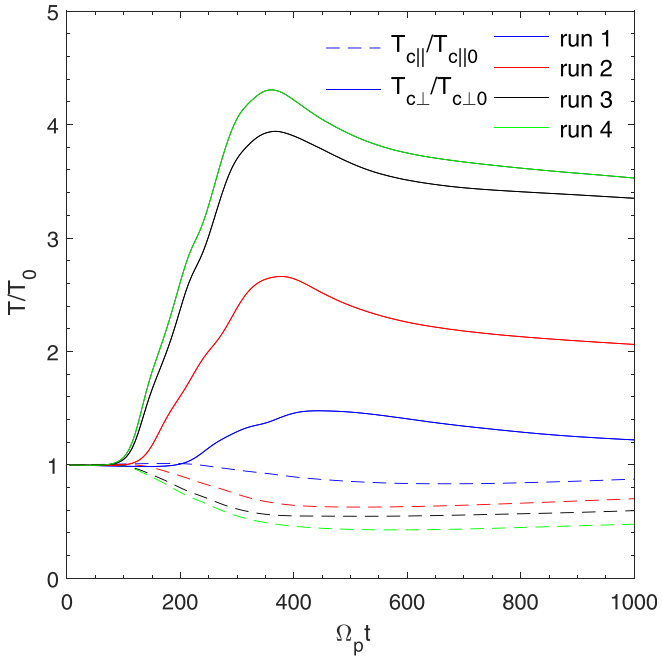

FIG. 5. The temporal profiles of the temperature of core protons. The blue, red, and black lines correspond to the temperature of core protons in run 1, run 2, and run 3, respectively. The solid lines and dashed lines denote perpendicular temperature and parallel temperature, respectively.

toward higher values, even exceeding the proton gyrofrequency. This results in more efficient heating of core protons in the perpendicular direction through the cyclotron resonance with Alfvén waves.

In addition, the effects of plasma beta and beam drift velocity on the instability and associated proton heating are also investigated. Just as expected, it is found that the higher beam drift velocity leads to larger amplitudes of waves and perpendicular temperature of core proton, while the larger plasma beta results in smaller amplitudes of waves and perpendicular temperature of core proton.

The perpendicular preferential heating of the core population in the solar wind is one of the most important topics of solar physics. The proton/proton instability has been considered as one of the promising mechanisms. Gao *et al.*[29] have pointed out that the proton/proton instability can excite the linearly polarized Alfvén waves, which can effectively heat core protons in the perpendicular direction. As a complementary work, we further study the effects of beam proportion on the electromagnetic proton/proton instability and associated proton heating, since the beam proportion is observed to be quite variable (10%–45%) in solar winds. Our results show that both the amplitude and peak frequency of excited oblique Alfvén waves increase with the beam proportion, and then the perpendicular heating of core protons via cyclotron resonance becomes more efficient. This study may promote our understanding of proton–proton instability and the heating of the solar wind. Moreover, the *Solar Probe Plus* mission, which is intended to collect *in situ* observations of the low solar corona,[44] could determine the role of proton–proton instability in solar wind heating via verifying the relationship between the beam proportion and the properties of accompanied Alfvén waves and associated perpendicular heating.

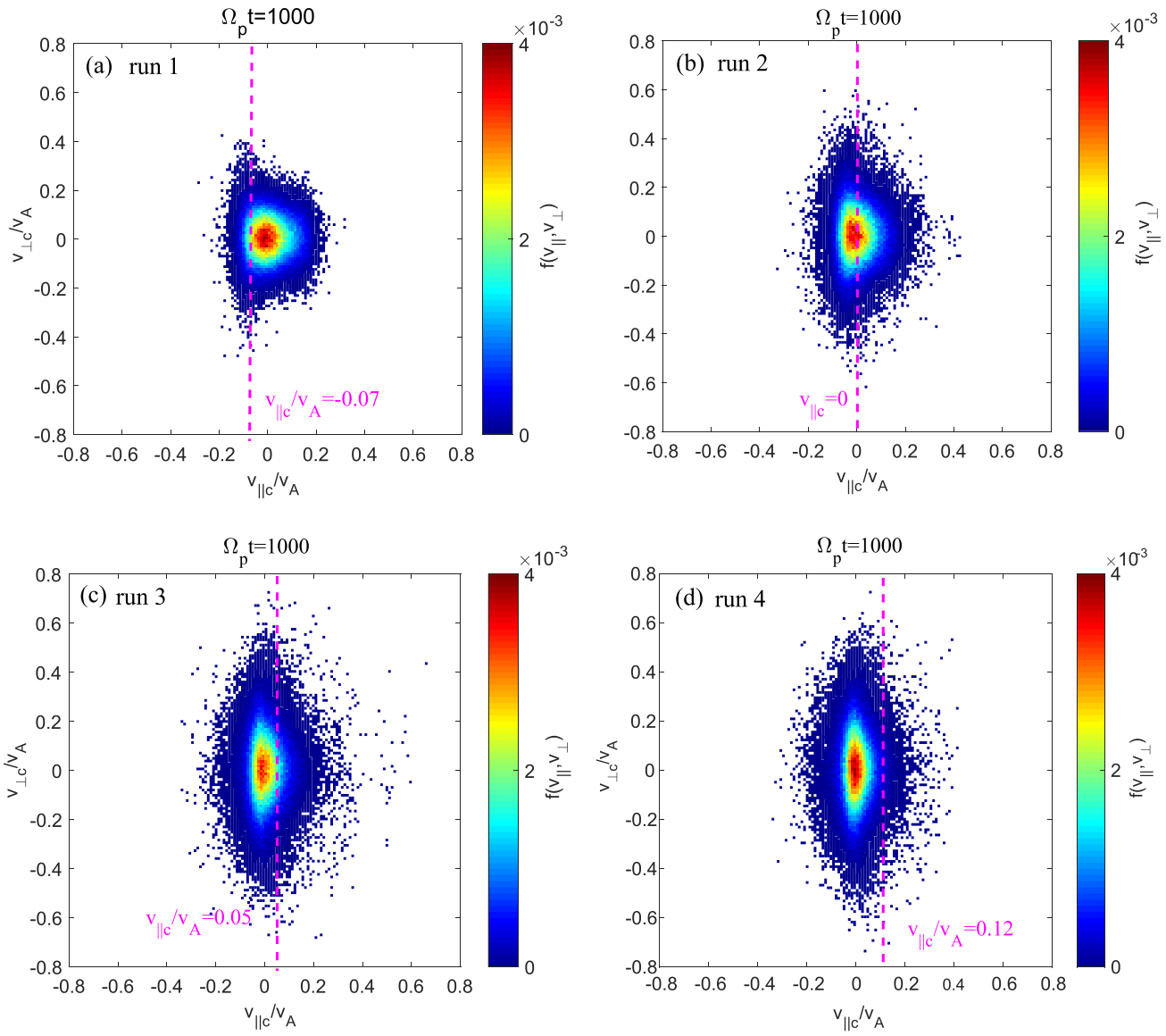

FIG. 6. The final velocity distributions in the $v_{\|c} - v_{\perp c}$ plane for (a) run 1, (b) run 2, (c) run 3, and (d) run 4 at $\Omega_p t \approx 1000$. Positions of magenta dashed lines are calculated via gyroresonance conditions, i.e., $v_{\|c} = (\omega - \Omega_p)/k_{\|c}$. Protons in the region on the left side of magenta dashed lines satisfy gyroresonance conditions and are scattered in the perpendicular direction.

ACKNOWLEDGMENTS

This work was supported by the NSFC Grant Nos. 41774151 and 41604128, Youth Innovation Promotion Association of Chinese Academy of Sciences (No. 2016395), and Young Elite Scientists Sponsorship Program by CAST (No. 2018QNRC001).

REFERENCES

[1]W. C. Feldman, J. R. Asbridge, S. J. Bame, and M. D. Montgomery, J. Geophys. Res. **78**, 2017, https://doi.org/10.1029/JA078i013p02017 (1973).
[2]W. C. Feldman, J. R. Asbridge, S. J. Bame, and M. D. Montgomery, Rev. Geophys. **12**, 715, https://doi.org/10.1029/RG012i004p00715 (1974).
[3]C. C. Goodrich and A. J. Lazarus, J. Geophys. Res. **81**, 2750, https://doi.org/10.1029/JA081i016p02750 (1976).
[4]E. Marsch, K.-H. Mühlhäuser, R. Schwenn, H. Rosenbauer, W. Pilipp, and F. M. Neubauer, J. Geophys. Res. **87**, 52, https://doi.org/10.1029/JA087iA01p00052 (1982).
[5]B. E. Goldstein, M. Neugebauer, L. D. Zhang, and S. P. Gary, Geophys. Res. Lett. **27**, 53, https://doi.org/10.1029/1999GL003637 (2000).
[6]C. Y. Tu, E. Marsch, and Z. R. Qin, J. Geophys. Res. **109**, A05101, https://doi.org/10.1029/2003JA010330 (2004).
[7]C. Y. Tu and E. Marsch, Sol. Phys. **171**, 363 (1997).
[8]J. V. Hollweg, J. Geophys. Res. **104**, 24781, https://doi.org/10.1029/1999JA900300 (1999).
[9]S. R. Cranmer, Astrophys. J. **532**, 1197 (2000).
[10]P. A. Isenberg, M. A. Lee, and J. V. Hollweg, J. Geophys. Res. **106**, 5649, https://doi.org/10.1029/2000JA000099 (2001).

[11]S. Sridhar and P. Goldreich, Astrophys. J. **432**, 612 (1994).
[12]P. Goldreich and S. Sridhar, Astrophys. J. **438**, 763 (1995).
[13]E. Quataert, Astrophys. J. **500**, 978 (1998).
[14]B. J. Vasquez, S. A. Markovskii, and B. D. G. Chandran, Astrophys. J. **788**, 178 (2014).
[15]J. He, C. Tu, E. Marsch, and S. Yao, Astrophys. J. Lett. **745**, L8 (2011).
[16]J. He, L. Wang, C. Tu, E. Marsch, and Q. Zong, Astrophys. J. Lett. **800**, L31 (2015).
[17]J. T. Gosling, S. J. Bame, W. C. Feldman, G. Paschmann, N. Sckopke, and C. T. Russell, J. Geophys. Res. **89**, 5409, https://doi.org/10.1029/JA089iA07p05409 (1984).
[18]L. Ofman, M. Balikhin, C. T. Russell, and M. Gedalin, J. Geophys. Res. **114**, A09106, https://doi.org/10.1029/2009JA014365 (2009).
[19]L. Chen, Z. H. Lin, and R. B. White, Phys. Plasmas **8**, 4713 (2001).
[20]Q. M. Lu and L. Chen, Astrophys. J. **704**, 743 (2009).
[21]Q. M. Lu and X. Li, Phys. Plasmas **14**, 042303 (2007).
[22]S. Jicheng, G. Xinliang, L. Quanming, and W. Shui, Plasma Sci. Technol. **16**, 919 (2014).
[23]X. L. Gao, Q. M. Lu, X. Li, C. Huang, and S. Wang, Phys. Plasmas **19**, 032901 (2012).
[24]H. Comisel, Y. Nariyuki, Y. Narita, and U. Motschmann, Ann. Geophys. **36**, 1647, https://doi.org/10.5194/angeo-36-1647-2018 (2018).
[25]X. L. Gao, Q. M. Lu, X. Li, and S. Wang, Phys. Plasmas **20**, 072902 (2013).
[26]X. L. Gao, Q. M. Lu, X. Tao, Y. F. Hao, and S. Wang, Phys. Plasmas **20**, 092106 (2013).
[27]Y. Nariyuki and T. Hada, Nonlinear Processes Geophys. **13**, 425 (2006).
[28]Y. Nariyuki, T. Hada, and K. Tsubouchi, J. Geophys. Res. **114**, A07102, https://doi.org/10.1029/2009JA014178 (2009).
[29]X. L. Gao, Q. M. Lu, X. Li, L. C. Shan, and S. Wang, Astrophys. J. **764**, 71 (2013).
[30]S. P. Gary, Space Sci. Rev. **56**, 373 (1991).
[31]S. P. Gary, M. E. McKean, and D. Winske, J. Geophys. Res. **98**, 3963, https://doi.org/10.1029/92JA02585 (1993).
[32]W. Daughton and S. P. Gary, J. Geophys. Res. **103**, 20613, https://doi.org/10.1029/98JA01385 (1998).
[33]W. Daughton, S. P. Gary, and D. Winske, J. Geophys. Res. **104**, 4657, https://doi.org/10.1029/1998JA900105 (1999).
[34]Q. M. Lu, A. Du, and X. Li, Phys. Plasmas **16**, 042901 (2009).
[35]L. Xiang, D. J. Wu, and L. Chen, Astrophys. J. **869**, 64 (2018).
[36]L. Xiang, D. J. Wu, and L. Chen, Astrophys. J. **857**, 108 (2018).
[37]D. Winske, Space Sci. Rev. **42**, 53 (1985).
[38]K. B. Quest, J. Geophys. Res. **93**, 9649, https://doi.org/10.1029/JA093iA09p09649 (1988).
[39]Q. M. Lu and S. Wang, Geophys. Res. Lett. **32**, L03111, https://doi.org/10.1029/2004GL021830 (2005).
[40]H. S. Xie, Comput. Phys. Commun. **244**, 343 (2019).
[41]L. Gomberoff and H. F. Astudillo, Planet. Space Sci. **46**, 1683 (1998).
[42]H. Sun, J. Zhao, H. Xie, and D. Wu, Astrophys. J. **884**(1), 44 (2019).
[43]P. He, X. L. Gao, Q. M. Lu, and S. Wang, Astrophys. J. **827**, 64 (2016).
[44]N. J. Fox, M. C. Velli, S. D. Bale, R. Decker, A. Driesman, R. A. Howard, J. C. Kasper, J. Kinnison, M. Kusterer, D. Lario *et al.*, Space Sci. Rev. **204**, 7 (2016).